



A numerical study of the bubble induced pressure fluctuation in gas-fluidized beds



Yuli Zhang^{a,b}, Rui Xiao^{a,*}, Mao Ye^{b,*}, Zhongmin Liu^b

^a Key Laboratory of Energy Thermal Conversion and Control of Ministry of Education, School of Energy and Environment, Southeast University, Nanjing 210096, China

^b Dalian National Laboratory for Clean Energy and National Engineering Laboratory for MTO, Dalian Institute of Chemical Physics, Chinese Academy of Sciences, Dalian 116023, China

ARTICLE INFO

Article history:

Received 26 May 2016

Received in revised form 7 August 2016

Accepted 24 August 2016

Available online 26 August 2016

Keywords:

Bubble size

Pressure fluctuation

Fluidized bed

Euler-Euler model

ABSTRACT

Pressure fluctuation analysis has been widely accepted as an efficient way for bubble size estimation in fluidized beds since the local bubble induced pressure fluctuation, which is believed to be a function of bubble size, can be separated away from the global pressure waves. The spectral data decomposition method developed by van der Schaaf et al. (2002) Van der Schaaf et al. (2002) has been widely used in this regard. However, it has been found in various experimental studies that the proportionality constant between the reference data (obtained via measurements by various techniques or predicted by well-established correlations) and the estimated bubble size differs significantly in different applications. In this work we try to understand the scattered proportionality constants via a numerical study based on the Euler-Euler two-fluid model. The simulation results indicate that the local bubble induced pressure fluctuation is affected not only by bubble size, but also by the lateral distance between the rising bubble and detecting point, bubble shape, bed diameter, and bubble coalescence. Without consideration of these factors, the spectral data decomposition method is subject to large deviation for bubble size estimation.

© 2016 Elsevier B.V. All rights reserved.

1. Introduction

Gas-fluidized beds have been widely used in the industry. Bubbles have been considered as the motor of fluidization, and the performance of a fluidized bed reactor can be well characterized by accurate estimation of the bubble parameters. In the past decades many techniques have been successfully applied in measuring bubble parameters in fluidized beds, like capacitance/optical fiber probes [1,2], X/γ-ray [3–5], and Electrical capacitance tomography [6,7]. Despite the applications in a diversity of processes, the aforementioned measuring technologies are mostly limited to ambient temperature and low pressure. Yet many fluidized bed reactors are running at high temperature and high pressure, and accurate measurement of bubble parameters under extreme conditions is relatively difficult.

The pressure fluctuation analysis [8] is one of the few measurement techniques suitable for fluidized beds operated under high pressure and high temperature. The in-bed pressure signal is a combination of the global fast compression waves and the local bubble induced slow pressure waves. The global fast compression waves originate from bubble eruption at the bed surface, bubble formation near the gas distributor, bubble coalescence, mechanical bed mass oscillations, gas fluctuations

in the windbox, and among others [9,10]. The passage of a bubble, referring to classical Davidson and Harrison model [11], can produce a local slow kinematic pressure wave with the amplitude proportion to the bubble size. Van der Schaaf et al. [12] proposed a spectral data decomposition method to obtain bubble size based on the different propagation velocity of the global and local pressure waves, in which the bubble induced local kinetic pressure wave information is first extracted from a coherence analysis of the pressure signal series detected simultaneously in the bed and in the windbox, and the bubble size is then inferred accordingly.

Though the spectral data decomposition method can well capture the bubble behavior in fluidized beds [13–16], it is challenged by its semi-quantitative nature in the bubble size estimation. The proportionality constant between the reference data (obtained via measurements by various techniques or predicted by well-established correlations) and the estimated bubble size (or called the characteristic length scale by van der Schaaf et al. [12]) differs significantly in different applications. Kleijn van Willigen et al. [17] reported in their 2D experiments that the proportionality constant is 1.3 for Geldart B particle and 8.1 for Geldart A particles. Rüdüsüli et al. [16] found the proportionality in the range of 2.0–8.0. The scattered proportionality constants apparently hinder the pressure fluctuation analysis as a robust measurement technique for quantitative bubble size estimation. The reasons underlying the large variation of the proportionality constants are yet to be understood.

* Corresponding author.

E-mail addresses: ruixiao@seu.edu.cn (R. Xiao), maoye@dicp.ac.cn (M. Ye).

The Euler-Euler two-fluid model, incorporated with the kinetic theory of granular flow (KTGF) [18,19] for formulating the rheologic parameters of particle phase, is capable of modeling gas-fluidized beds effectively [18–21]. Particularly, it can be used as a learning tool for studying the complicate hydrodynamic phenomena which are difficult to measure with advanced instruments. In this work, we try to understand the reason underlying the large variation of the proportionality constants in gas-fluidized beds by use of the Euler-Euler two-fluid model, in which both the bubble size and pressure fluctuation signal can be directly retrieved. To this end, the spectral data decomposition method by Van der Schaaf et al. is first validated and evaluated by the simulation results. Since the simulation results can correlate bubble size and the corresponding pressure fluctuation signals in a direct way, we then analyze the underlying reasons for the large variation of the proportionality constant. A detailed discussion on the scattered proportionality constants in bubble size estimation from pressure fluctuation signals is given out. And last this paper is concluded with some suggestions on improving bubble size estimation via pressure fluctuation analysis.

2. Model descriptions

In the Euler-Euler two-fluid model, both the gas and particle phase are considered as continuous medium and described by volume-averaged Navier-Stokes equations. The relevant equations are listed in Table 1. The rheologic properties of the fluidized particles formulated by the kinetic theory of granular flows (KTGF) are used to achieve the closures of the governing equations for particle phase [18,19]. The granular viscosity and granular conductivity are calculated by use of the expressions by Gidaspow et al. [18]. The solid phase pressure, the radial distribution, and the granular bulk viscosity are proposed by Lun et al. [19]. The frictional viscosity of the solid phase is according to that by Johnson and Jackson [22]. The inter-phase momentum transfer coefficient is obtained via the correlation of Wen and Yu [23] for dilute regime, and Ergun [24] equation for dense regime. The boundary conditions follow that by Sinclair and Jackson [25], where a no-slip boundary condition is used for gas phase while a half slip boundary condition for particle phase, with the specular coefficient of 0.25 and restitution coefficient of 0.2.

Table 1
Equations of the Euler-Euler two-fluid model.

The continuity equations: For gas phase $\frac{\partial(\epsilon_g \rho_g)}{\partial t} + \nabla \cdot (\epsilon_g \rho_g \vec{u}_g) = 0$ For particle phase $\frac{\partial(\epsilon_s \rho_s)}{\partial t} + \nabla \cdot (\epsilon_s \rho_s \vec{u}_s) = 0$ The momentum equations: For gas phase $\frac{\partial(\epsilon_g \rho_g \vec{u}_g)}{\partial t} + \nabla \cdot (\epsilon_g \rho_g \vec{u}_g \vec{u}_g) = -\epsilon_g \nabla p + \nabla \cdot \overline{\overline{\tau}}_g + \epsilon_g \rho_g \vec{g} - \beta(\vec{u}_g - \vec{u}_s)$ For particle phase $\frac{\partial(\epsilon_s \rho_s \vec{u}_s)}{\partial t} + \nabla \cdot (\epsilon_s \rho_s \vec{u}_s \vec{u}_s) = -\epsilon_s \nabla p - \nabla p_s + \nabla \cdot \overline{\overline{\tau}}_s + \epsilon_s \rho_s \vec{g} + \beta(\vec{u}_g - \vec{u}_s)$ The Granular temperature equation: $\frac{3}{2} \left\{ \frac{\partial(\epsilon_s \rho_s \theta)}{\partial t} + \nabla \cdot (\epsilon_s \rho_s \vec{u}_s \theta) \right\} = -(\rho_s \vec{I} + \overline{\overline{\tau}}_s) : \nabla \vec{u}_s + \nabla \cdot (k_s \nabla \theta) - \gamma_s - 3\beta \theta$ The inter-phase momentum transfer coefficient β : $\beta = \begin{cases} \frac{4}{3} C_D (1 - \epsilon_g) \epsilon_g \rho_g \vec{u}_g - \vec{u}_s \\ \frac{d_p \epsilon_g^{-2.65}}{d_p \epsilon_g^{-0.8}} \cdot \frac{\epsilon_g \geq 0.8150 (1 - \epsilon_g)^{1.5} \rho_g \cdot \frac{1}{4} (1 - \epsilon_g) \mu_g \vec{u}_g - \vec{u}_s }{\epsilon_g d_p^2} \end{cases}$ where $C_D = \begin{cases} \frac{24}{Re} (1 + 0.15 Re^{0.687}), & Re < 1000 \\ 0.44, & Re \geq 1000 \end{cases}$ $Re = \epsilon_g \rho_g \vec{u}_g - \vec{u}_s d_p$
--

3. Simulation setup

The modeling approach described above has been implemented into the commercial CFD code, Fluent 6.3. The simulations were carried out for 2D fluidized beds. As illustrated in Fig. 1, three reactors with different sizes were used in the simulations:

Reactor I: 2D fluidized bed reactor with a width of 0.15 m, height of 0.8 m, and initial bed height of 0.5 m;

Reactor II: 2D fluidized bed reactor with a width of 0.5 m, height of 1.5 m, and initial bed height of 1.0 m;

Reactor III: 2D fluidized bed reactor with a width of 0.15 m, height of 1.5 m, and initial bed height of 0.8/1.0 m;

In order to evaluate the spectral data decomposition method, *Reactor I* (cf. Fig. 1 (a)) is used for simulation of freely bubbling fluidized bed with a uniform gas velocity at the inlet. *Reactor II* and *Reactor III*, as displayed in Fig. 1 (b), are used for simulation of single-bubble or twin-bubble to find the reasons underlying the large variation of the proportionality constants. Single bubble was injected into *Reactor II* and *Reactor III* operated at incipient fluidization through a central jet orifice. The width of the central jet orifice, as shown in Fig. 1 (b), is 0.005 m. The injected bubble size can be controlled by altering the jetting velocities. The labels a, b and c in Fig. 1 (b) are the detecting points for pressure signals, representing different radial distances between the detecting point and the bubble centerline. The grid dependence was first examined for these three reactors. A computational grid with uniform grid size of 0.0025 m × 0.0025 m and a time step of 1 × 10⁻⁴ s were used in all simulations. Typical parameters describing the particle properties and operating conditions are listed in Table 2.

4. Data processing

4.1. Bubble size from the spectral data decomposition method

In the bubbling fluidized bed simulations, the sampling frequency for the pressure signals here is 1000 Hz, with a total number of data points of 61,440 (61.44 s) chosen from each measurement. And each time series is divided into 30 segments with each subset of 2048 data points for spectral analysis. According to the spectral data decomposition method by Van der Schaaf et al. [12], the coherence between the two time series of pressure signals at the gas distributor and in the bed is first analyzed:

$$C_{XY}^2(f) = \frac{\varphi_{XY}(f) \cdot \varphi_{XY}^*(f)}{\varphi_{XX}(f) \cdot \varphi_{YY}(f)} \quad (1)$$

where $\varphi_{XX}(f)$ is the power spectral density (PSD) of the pressure time series at the gas distributor, $\varphi_{YY}(f)$ is PSD of the in-bed pressure time series, and $\varphi_{XY}(f)$ is the cross PSD for the two time series.

The coherence ranges from 0 to 1. A coherence of 1 means that the time series are totally coupled while a coherence of 0 means not coupled. Owing to the absence of bubbles, the time series of pressure fluctuations at the gas distributor only contain the global pressure fluctuations. While the pressure fluctuations in the bed are composed of the global pressure fluctuations and the local pressure fluctuation due to bubble passage. Hence the coherent part between the two is the global ones while the incoherent part is the local ones. Then $\varphi_{YY}(f)$ is further divided into a coherent output PSD (refer to $COP_{XY}(f)$) and incoherent output PSD (refer to $IO_{XY}(f)$) by the coherence, which correspond to the global fast compression waves and bubble passage induced local pressure fluctuations, respectively:

$$COP_{XY}(f) = C_{XY}^2(f) \cdot \varphi_{XX}(f) \quad (2)$$

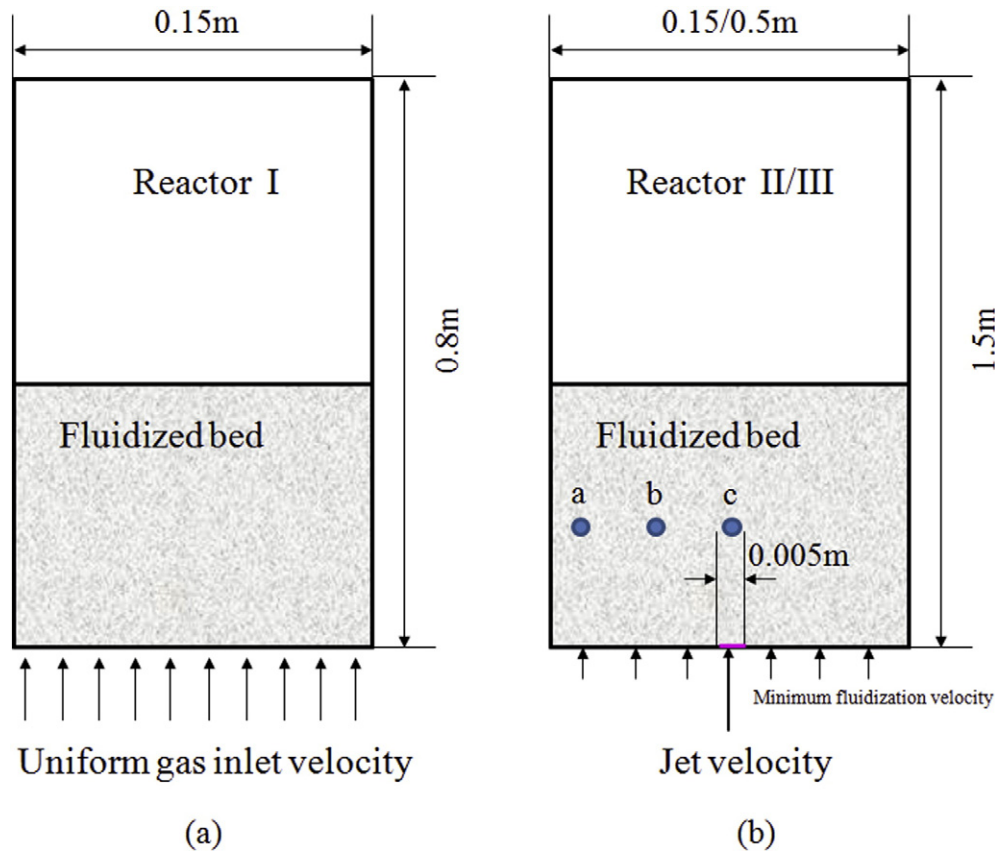


Fig. 1. The schematic diagrams of fluidized bed Reactors used in the simulations. (a) Reactor I with uniform gas inlet velocity; (b) Reactor II and Reactor III with a central gas jet and the labels a, b, c represent the detecting points for pressure signals.

$$IOP_{XY}(f) = (1 - C_{XY}^2(f)) \cdot \varphi_{XX}(f) \quad (3)$$

Last the bubble size (or characteristic length scale) is calculated:

$$L_b = \frac{\sigma_{IOP}}{(\rho_p - \rho_g)g(1 - \varepsilon)} \quad (4)$$

where σ_{IOP} is the standard deviation of $IOP_{XY}(f)$, ρ_p is the particle density, ρ_g is the gas density, and ε is the voidage of the emulsion phase.

4.2. Bubble size from the local pressure fluctuations due to single bubble passage

When a single bubble rises through a bed at minimum fluidization, the pressure fluctuation induced by bubble formation, bubble passage, and bubble eruption at the bed surface can be separately distinguished from each other (cf. Fig. 9). In analogy to the theory of the spectral data

decomposition method, the bubble size can be directly calculated from the local pressure fluctuations:

$$l_b = \frac{\sigma_{local}}{(\rho_p - \rho_g)g(1 - \varepsilon)} \quad (5)$$

where σ_{local} is the standard deviation of the local pressure fluctuations due to bubble passage.

4.3. Bubble size from voidage distribution

A void fraction cutoff of 0.75 is chosen to distinguish the boundary between the bubble phase and the emulsion phase for calculating the bubble size from voidage distributions. The bubble equivalent diameter a bubble can be calculated as

$$D_b = 2\sqrt{\frac{A}{\pi}} \quad (6)$$

where A is the total area occupied by a 2D bubble.

For bubbling fluidized bed, the mean bubble size at a specific bed height is calculated by

$$\bar{D}_b = \frac{\sum_{i=1}^n D_{b,i}}{n} \quad (1 \leq i \leq n) \quad (7)$$

where n is the number of bubble used for average and $D_{b,i}$ the equivalent diameter of the number i bubble passing by a specific bed height.

Table 2
Typical parameters used in the simulations.

Parameters	Value
Particle diameter, [μm]	460
Particle density, [kg/m^3]	2660
Restitution coefficient, [–]	0.95
angle of the internal friction, [$^\circ$]	30
Gas density, [kg/m^3]	1.225
Gas viscosity, [$\text{Pa}\cdot\text{s}$]	1.8×10^{-5}
Solid volume fraction at minimum fluidization condition, [–]	0.63
Minimum fluidization velocity, [m/s]	0.165

4.4. Proportionality constant

In the literature, the proportionality constant is defined as the ratio between the reference data (obtained via measurements by various techniques or predicted by well-established correlations) and the characteristic length scale by the spectral data decomposition method. In this study, the proportionality constant is defined as follows:

For simulation of bubbling fluidized bed:

$$\text{Proportionality constant} = \frac{\overline{D_b}}{L_b} \quad (8)$$

and for simulation of a single bubble:

$$\text{Proportionality constant} = \frac{D_b}{l_b} \quad (9)$$

5. Results and discussion

5.1. Freely bubbling fluidized bed

For the validation and evaluation of the spectral data decomposition method by van der Schaaf et al. [12], the bubble behavior in a freely bubbling fluidized bed is first numerically investigated here. Fig. 2 shows the typical transient bubbling flow patterns at different superficial velocities when the simulations reach a quasi-steady-state. It shows an apparent increase of bubble size with increasing the superficial velocity. Fig. 3 demonstrates an example of pressure fluctuation signals

simultaneously measured at different bed heights above the gas distributor at a superficial velocity of $U_{\text{mf}} + 0.23$ m/s. The power spectral distributions of the original pressure series in Fig. 3 are plotted in Fig. 4 (a). Following van der Schaaf et al., a coherent analysis is performed between pressure fluctuation series at a specific bed height and at the gas distributor. Fig. 4 (b) plots out the coherence, $C_{XY}^2(f)$, between the pressure signal in the bed and at the gas distributor. Van der Schaaf et al. [10] found that the downward traveling global pressure waves have minor attenuation while the upward traveling ones decay linearly to zero along the bed height. Thereby the attenuation of the upward traveling global pressure waves and the growth of bubble size with increasing the bed height result in a decrease of coherence along the bed height. With the coherence in Fig. 4 (b), the PSDs in Fig. 4 (a) are separated into a coherent-output PSDs (COPs) and incoherent-output PSDs (IOPs), as displayed in Fig. 4 (c) and Fig. 4 (d), respectively.

Fig. 5 (a) shows the average bubble size (characteristic length scale) derived from the standard deviation of the IOPs by Eq. (4). It can be seen from Fig. 5 (a) that the bubble growth cannot be appropriately characterized when the bed height is higher than 0.4 m. Van der Schaaf et al. attributed this to that the bed material above the bubble is not enough to achieve the complete bubble-induced local pressure curve. Thereby only the bubble sizes from pressure signals below the bed height of 0.4 m can be used to compare with the mean bubble size (real bubble size) calculated from voidage distribution. The left axis of Fig. 5 (b) illustrates the mean bubble diameters calculated from voidage distribution by Eq. (7) as well as that predicted from literature correlations (Darton [26], Cai et al. [27], and Shen et al. [28], details are listed in Table 3) at the bed height of 0.3 m above the gas distributor. It can be seen from Fig. 5 (b) that the mean bubble size calculated from voidage distribution stays

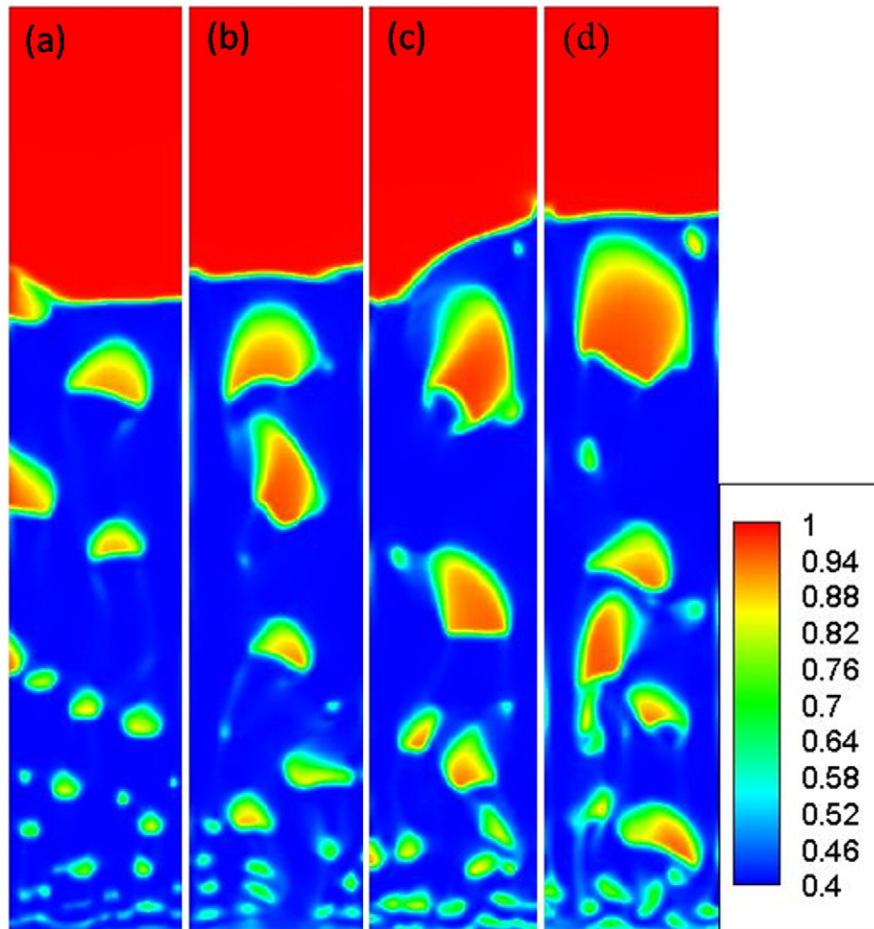


Fig. 2. Snapshots of bubbling flow patterns in Reactor I ($W \times H$: 0.15 m \times 0.8 m) at different superficial velocities: (a) $U - U_{\text{mf}} = 0.08$ m/s, (b) $U - U_{\text{mf}} = 0.13$ m/s, (c) $U - U_{\text{mf}} = 0.18$ m/s, (d) $U - U_{\text{mf}} = 0.23$ m/s.

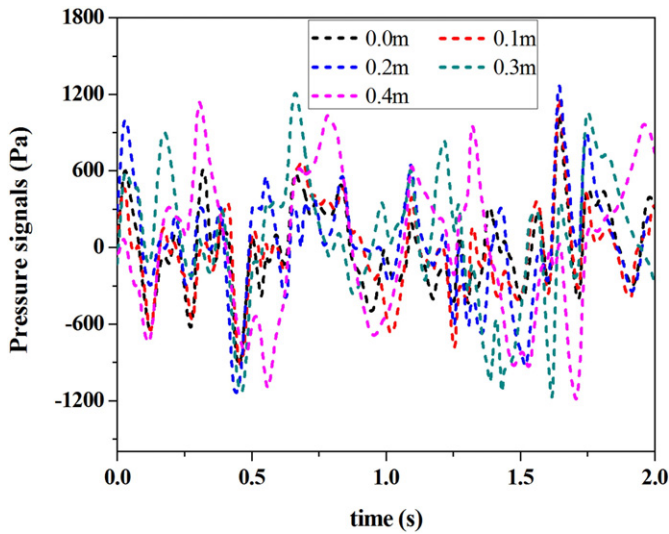


Fig. 3. Original pressure signals simultaneously detected at different bed heights above the gas distributor, $U - U_{mf} = 0.23$ m/s.

in the middle among the three empirical equations, indicating that the CFD model used here can well estimation the bubble size in a bubbling fluidized bed. The right axis of Fig. 5 (b) plots the proportionality constant between the bubble size from the voidage distribution and the spectral data decomposition method at the bed height of 0.3 m. It can be seen from the right axis of Fig. 5 (b) that the proportionality constant decreases gradually from 5.65 to 2.94 while the superficial velocity

increases from $U_{mf} + 0.08$ m/s to $U_{mf} + 0.23$ m/s, showing the same varying pattern with the experimental results by Rüdüsüli et al. [16]. Accordingly, the estimated bubble size from the spectral data decomposition method is obvious much smaller than the actual one.

When a bubble passes through the cross section of observation, both local pressure and local solid holdup in the cross section will vary periodically. Apparently the amplitude of the two kinds of time series should be both proportional to the bubble size. If the spectral data decomposition method can successfully extract out the local pressure fluctuations, the two time series should share the similar shape of the PSDs, with a major frequency related to the local bubble frequency. Fig. 4 (d) and Fig. 6 displayed the incoherent part of PSDs (IOPs) of pressure fluctuations and PSDs of the solid holdup fluctuations in the whole cross section, respectively. It can be clearly seen that, the shape of PSDs of the local solid holdup fluctuations agrees well with that of IOPs in Fig. 4 (d) at each bed height. This good agreement clearly confirms that, the method proposed by van der Schaaf et al. can effectively separate out the local bubble passage induced pressure fluctuation signals away from the global ones. Hence it needs to understand the large diversity of proportionality constant. To this purpose, we focused on the single bubble or twin bubbles in a fluidized bed under minimum fluidization condition, by which detailed analysis on the relationship between the bubble and the corresponding local pressure fluctuations can be easily carried out.

5.2. Single bubble

In this section, single bubble induced pressure fluctuations in fluidized bed will be first studied, in order to capture the reasons underlying the large variation of the proportionality constants in the spectral data

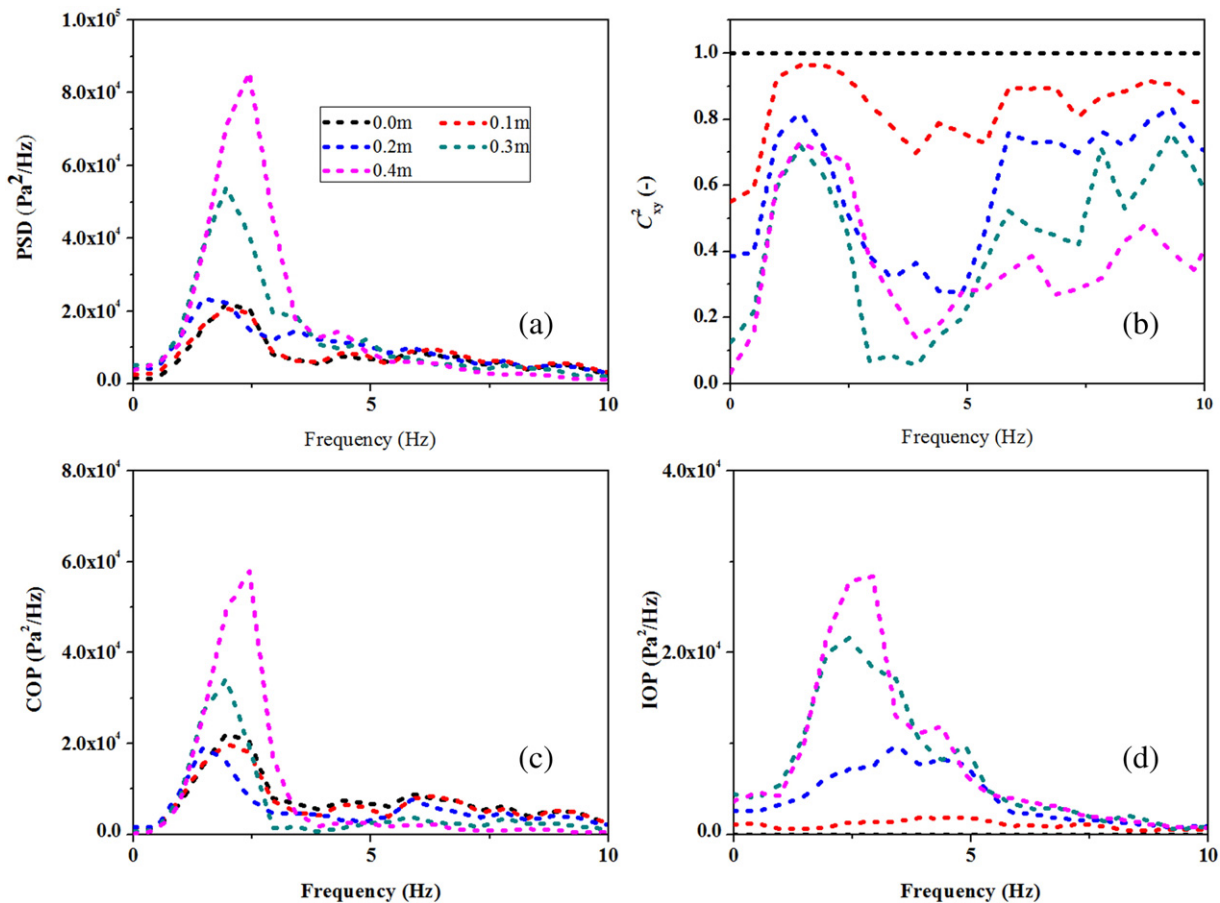


Fig. 4. Spectral distribution of time series at different measurement heights with a superficial velocity of $U_{mf} + 0.23$ m/s. (a) The PSDs of pressure signals in Fig. 3; (b) The coherence of pressure signals at different measurement heights with that at the gas distributor; (c) The coherent part in the PSDs, COPs; (d) The incoherent part in the PSDs, IOPs.

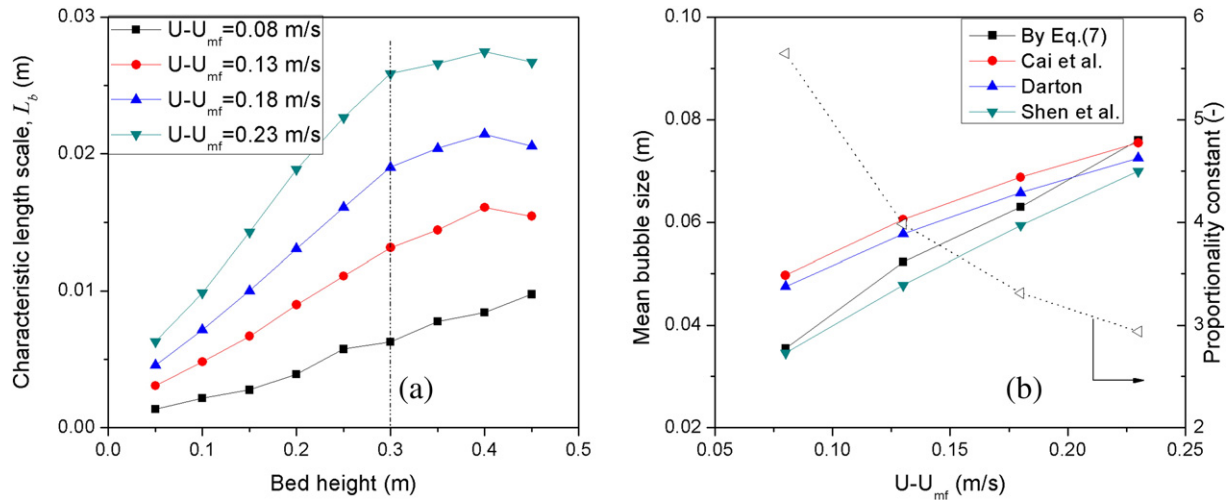


Fig. 5. (a) Bubble size, versus the measuring bed height at different gas inlet flow rates, calculated by the spectral data decomposition method. (b) Left axis: Bubble size predicted by voidage distribution and literature bubble growth correlations from Darton et al., Cai et al., and Shen et al. at the bed height of 0.3 m.; Right axis: The proportionality constant calculated by Eq. (7) (the hollow triangle) at the bed height of 0.3 m.

decomposition method. A bubble size of 0.075 m was injected into *Reactor II* through the following process: The gas velocity from the distributor is initially set to the minimum fluidization velocity and maintained for a certain time until the bed was fully fluidized. Then the gas velocity in the central jet orifice is prompted to 8 m/s and kept for 0.11 s. After the gas bubble is successfully injected, the gas velocity in the center jet orifice is switched back to the minimum fluidization velocity. On the other hand, single bubble rising in *Reactor III* with size of 0.075 m, 0.055 m, and 0.046 m were considered in three separate simulation cases.

5.2.1. Relative pressure distribution around a single bubble

Fig. 7 illustrates the rising process of the single bubble in *Reactor II*. It can be seen from Fig. 7 (a–c) that the evolution of the bubble wake deforms the introduced spherical bubble to a spherical cap shape when it rises in the fluidized bed. Fig. 7 (d–f) depicts the pressure contours in the fluidized bed, where the local pressure fluctuations due to the presence of bubble can be clearly identified.

In an early experimental work by Littman and Homolka [29], the normalized relative pressure distribution around a rising bubble in a pseudo-2D fluidized bed was reported. The size of *Reactor II* in Fig. 7 has the same size with that pseudo-2D column and the particle properties are also similar. Accordingly, our simulation results are compared with the experimental results. Fig. 8 compares the normalized pressure curve obtained in this simulation with the experimental results of Littman and Homolka [29] and the theoretical prediction by the Davidson and Harrison model [11]. The Davidson and Harrison model is a theoretical model that describes the relative pressure distributions around a single bubble in the fluidized beds:

For a 2D bubble

$$P_r = \begin{cases} (\rho_p - \rho_g)g(1-\varepsilon)\frac{R_b^2}{r} \cos\theta & \text{for } r > R_b \\ (\rho_p - \rho_g)g(1-\varepsilon)r \cos\theta & \text{for } r \leq R_b \end{cases} \quad (10)$$

for a 3D bubble

$$P_r = \begin{cases} (\rho_p - \rho_g)g(1-\varepsilon)\frac{R_b^3}{r^2} \cos\theta & \text{for } r > R_b \\ (\rho_p - \rho_g)g(1-\varepsilon)r \cos\theta & \text{for } r \leq R_b \end{cases} \quad (11)$$

Fig. 8 shows the normalized relative pressure distribution along three different vertical axes with parallel distances of 0, R_b and $2R_b$ from the bubble centerline, respectively. As can be seen in Fig. 8, the simulated results agree well with the Littman and Homolka's experimental results [29] for all three cases, indicating that the Euler-Euler two-fluid model can well simulate the pressure distribution in fluidized beds. A close check with the theoretical predictions by the Davidson and Harrison model, however, suggests that it deviates from the simulation results in this work (and also the experimental results by Littman and Homolka). It can be found in Fig. 8 (a–c) that the deviation mainly occurs in the zone below the center of rising bubble, i.e. the zone with $Z/R_b < 0$, and the deviation is more pronounced in case of a larger parallel distance from the bubble centerline. It is indeed not surprising as the Davidson and Harrison model was originally derived for well-developed spherical bubble. Yet the gas bubbles in a real fluidized bed reactor are not exactly spherical. In Fig. 7, the gas bubble has the shape of spherical cap due to the formation of wake in gas bubbles. The Davidson and Harrison model, therefore, cannot well describe the pressure fluctuation around real bubble when the bubble shape differs significantly from spherical. As an intrinsic feature of bubbling fluidized beds, the formation of wake in a gas bubble will deform the gas bubble to a non-spherical shape, which complicates the local bubble induced pressure fluctuation.

5.2.2. Single-point pressure fluctuation in the fluidized beds

The detecting points at the same bed height are recorded simultaneously (marked as point a–c in Fig. 1b). Fig. 9 displays three time series of the normalized single-point pressure signals recorded at a bed height

Table 3

Literature correlations for bubble size in bubbling fluidized bed.

$$\begin{aligned} \text{Darton : } d_b(z) &= \frac{0.54(u_0 - u_{mf})^{0.4} (h + 4\sqrt{A_0})^{0.8}}{g^{0.2}} \\ \text{Cai : } d_b(z) &= 0.38h^{0.8} (U - U_{mf})^{0.42} \exp[-0.25(U - U_{mf})^2 - 0.1(U - U_{mf})] \\ \text{Shen : } d_b(z) &= \frac{0.89(u_0 - u_{mf})(h + 3.0A_0/\delta)^{2/3}}{g^2} \end{aligned}$$

A_0 is the area of distributor per orifice and the value is set to zero here.

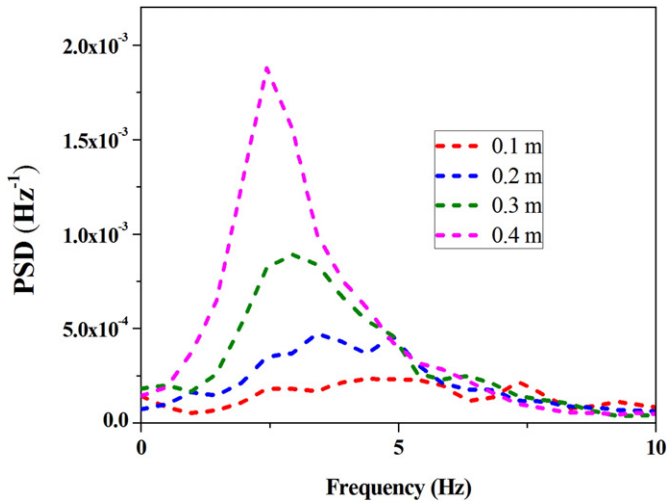


Fig. 6. The power spectral distributions of the time series of solid fraction in the whole cross section at different bed heights, $U - U_{mf} = 0.23$ m/s.

of 0.5 m above the gas distributor during the single bubble rising through *Reactor II*. Such time series were also derived by Littman and Homolka [29] and van der Schaaf et al. [10] in their experimental work. As displayed in Fig. 9, three sources of pressure fluctuations could be separately distinguished from the time series: the first phase originates from the bubble formation and homogeneous oscillation, the second phase is the bubble passage induced local pressure fluctuations when the bubble gets closer to the detecting point, and the third one corresponds to the bubble eruption at the bed surface [10].

In analogy to the spectral data decomposition method by van der Schaaf et al., the bubble size is calculated by the standard deviation of bubble induced local pressure fluctuations. The bubble in Fig. 9 arrived at the height of the detecting points (0.5 m above the gas distributor) at the time of 0.85 s. The bubble size is calculated from the standard deviation of the time series of pressure fluctuations ranging from 0.5 s to 1.5 s in Fig. 9 by Eq. (5), as displayed in Fig. 10. It can be seen from Fig. 10 that the bubble size/proportionality constant estimated from the pressure fluctuation is dependent on the lateral distance between the

detecting point and the center axis of bubble. The derived bubble size decreases with increasing the lateral distance between the detecting point and the center axis of bubble. Thereby a higher proportionality constant can be found with a larger lateral distance.

For comparative analysis, we also introduced bubble size of 0.075 m *Reactor III*. It can be clearly seen from Fig. 10 that, given a bubble with diameter of 0.075 m, the bubble size calculated from the pressure analysis in *Reactor III* is larger than that in *Reactor II*. This can be explained as follows. In Fig. 9, the starting point (time $t = 0$) represents the instant when the bubble was jetted, and the bed pressure measured at the corresponding detecting point is P_0 . After the gas bubble is introduced into the fluidized bed, more bed material (with the same volume with the introduced bubble) is lifted to above the corresponding detecting point and the bed pressure is then elevated to P_1 . The additional bed pressure ΔP can be estimated by [30]:

$$P_1 - P_0 = \frac{\Delta P}{(\rho_p - \rho_g)g(1 - \epsilon)} = \begin{cases} \frac{A}{2R_B} = \frac{\pi R_b}{2} \left(\frac{R_b}{R_B}\right)^2 & \text{for 2D bed} \\ \frac{V}{\pi R_B^2} = \frac{4R_b}{3} \left(\frac{R_b}{R_B}\right)^3 & \text{for 3D bed} \end{cases} \quad (12)$$

where R_B is the bed diameter, A the area of a 2D bubble and V the volume of a 3D bubble.

After the bubble passing the corresponding detecting point, the pressure measured at this detecting point is expected to return to the initial pressure P_0 . Accordingly, the local kinetic pressure fluctuation signal induced by bubble will contain: one is the relative pressure fluctuation as displayed in Fig. 8, and another is the reduced hydrostatic head after bubble passing, ΔP . According to Eq. (12), for a given bubble size, ΔP will be smaller in a wider bed, resulting in smaller amplitude of pressure fluctuations. Hence the bubble size calculated from pressure fluctuations is also determined by the size of the fluidized bed.

We introduced bubble with different bubble sizes into *Reactor III* in three separate simulation cases. As displayed Fig. 10 (b), the proportionality constant decrease with increasing the actual bubble diameter in the same fluidized bed. Taking a 2D bubble as example, the corresponding local pressure fluctuation is a combination of P_r in Eq. (10) and ΔP in Eq. (12) where the amplitude of P_r is proportional to the bubble radius and ΔP is proportional to the radius squared. Therefore, the

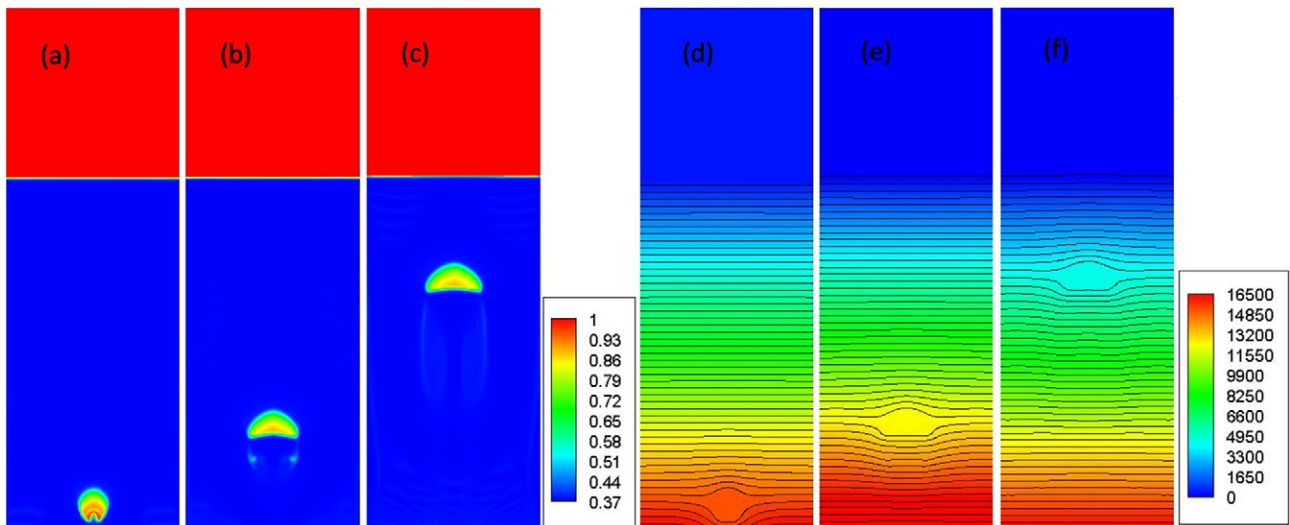


Fig. 7. The evolution of the gas voidage distribution (a–c) and the pressure field (d–f) in the fluidized bed (0.5 m × 1.5 m, *Reactor II*) after a bubble injected into the bed. The gas jet velocity is 8 m/s and jet duration is 0.11 s.

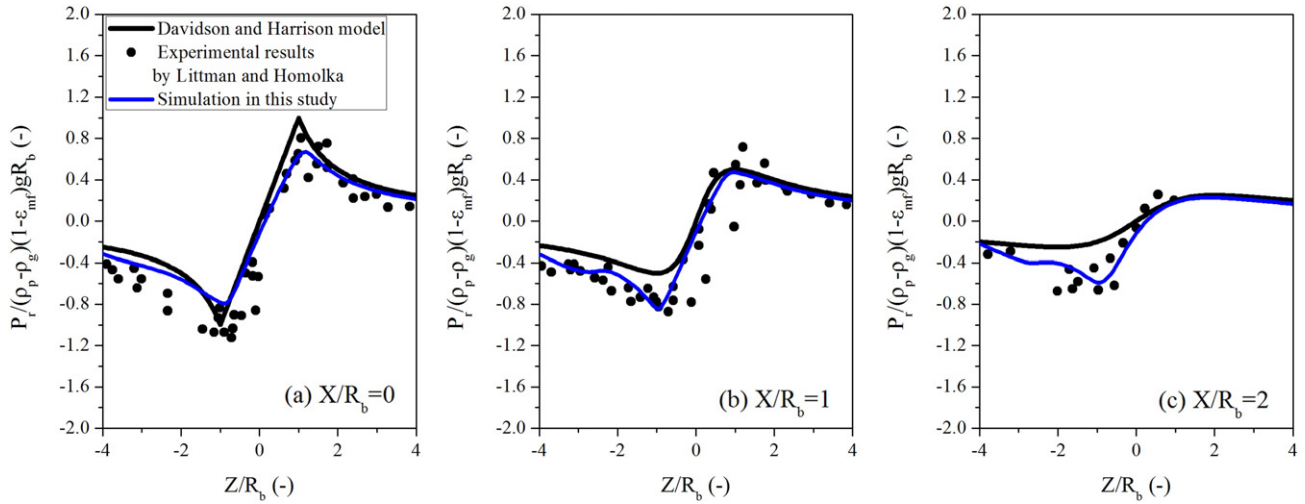


Fig. 8. Normalized relative pressure along different vertical axes parallel to the central axis of the rising bubble in Fig. 7(b), where the parallel distances are 0 for (a), R_b for (b), and $2R_b$ for (c), respectively.

proportionality constant in Eq. (9) can be represented as

$$\begin{aligned}
 \text{Proportionality constant} &= \frac{D_b}{l_b} = \frac{D_b}{\frac{\sigma_{local}}{(\rho_p - \rho_g)g(1-\varepsilon)}} \\
 &= \frac{D_b}{\frac{K_1 R_b + K_2 R_b^2}{(\rho_p - \rho_g)g(1-\varepsilon)}} = \frac{D_b}{\frac{0.5K_1 D_b + 0.25K_2 D_b^2}{(\rho_p - \rho_g)g(1-\varepsilon)}} \\
 &= \frac{(\rho_p - \rho_g)g(1-\varepsilon)}{0.5K_1 + 0.25K_2 D_b}
 \end{aligned}
 \tag{13}$$

where K_1 and K_2 are the constants. It can be directly seen from the Eq. (13) that the proportionality constant is inversely proportional to D_b . And then the bubble size calculated from pressure fluctuations is less underestimated with a larger bubble.

5.3. Two coalescing bubbles

In real bubbling fluidized beds, frequent bubble coalescence will lead to bubble growth along the bed height. The influence of bubble

interaction on bubble induced local pressure fluctuations is investigated in this section. Two successive bubbles are introduced into *Reactor III*. The gas velocity in the central jet orifice is prompted to 6 m/s and kept for 0.1 s to generate the first bubble. Then the gas velocity in the center jet orifice was switched to the minimum fluidization velocity. After 0.25 s, a second bubble was injected into the bed with the same jetting velocity (6 m/s) and jetting duration of 0.08 s. Then the gas velocity in the center jet orifice was switched to the minimum fluidization velocity again. Fig. 11 shows the rising and coalescence process of two bubbles. It can be clearly seen from Fig. 11 that before coalescence the second bubble has a higher aspect ratio (bubble height to width ratio) and larger rising velocity due to the drag from the first bubble. When these two bubbles approach, the second bubble gets into the wake of the first bubble, and the two bubbles coalesce into a bigger bubble at the time of about 0.95 s and bed height of 0.4 m.

Fig. 12 displays the simulation results of time series of pressure signals at different bed heights above the gas distributor in *Reactor III*. All the detecting points have been placed at different elevations on the vertical axis through the bubble centre. Comparing Fig. 9 with Fig. 12, the pressure fluctuation due to bubble formation, bubble passage and bubble eruption can be distinguished at detecting points of different elevations in the fluidized bed. In addition to that, displayed in Fig. 12 (b) as

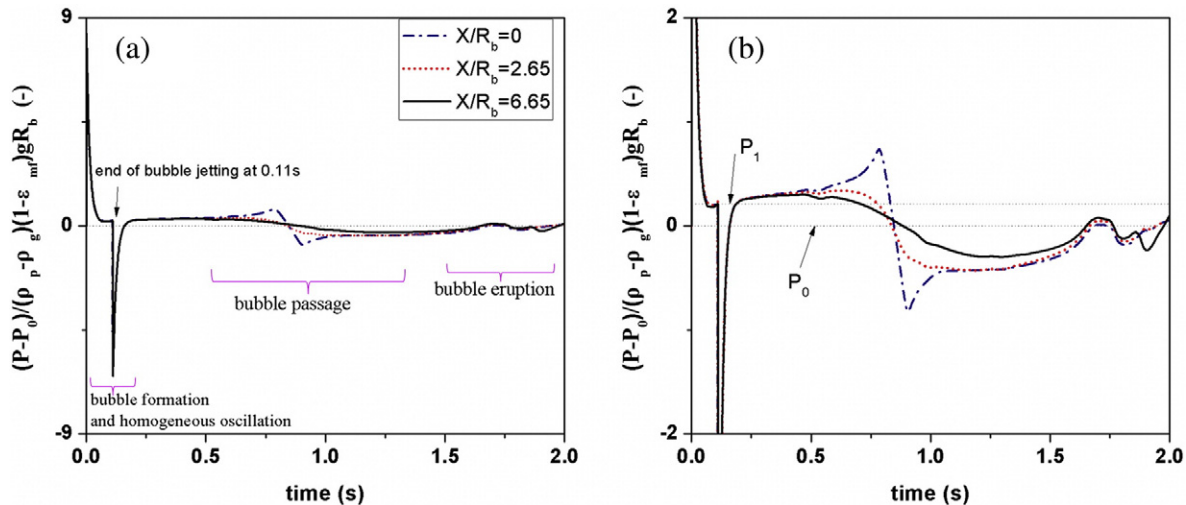


Fig. 9. (a) Time series of the normalized single-point pressure fluctuations at 0.5 m above the gas distributor in the 2D fluidized bed (*Reactor II*), (b) Details of (a). X is the radial distance between the detecting points and the bubble centerline.

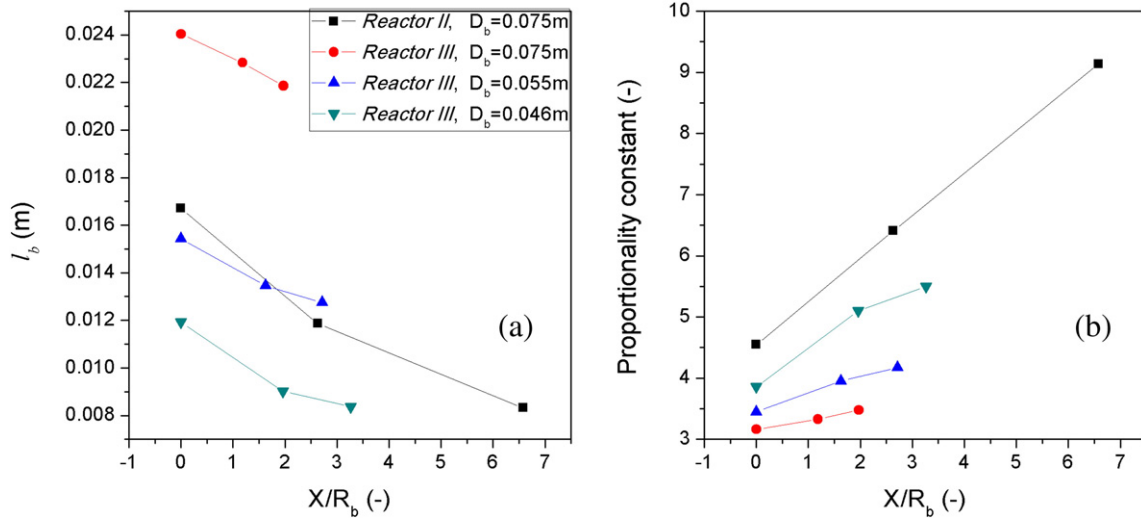


Fig. 10. (a) bubble size calculated from pressure fluctuations due to bubble passage by Eq. (5); (b) proportionality constants by Eq. (9). D_b is the bubble diameter introduced into fluidized bed at minimum fluidization condition.

another synchronous pressure fluctuation signals are also captured at the time of about 0.95 s. Fig. 13 shows the instant of twin-bubble coalescence and corresponding flow time, where it can be readily captured that the bubble coalescence just occurred at the time between 0.90s and 0.98 s, just the time when the forth source of pressure fluctuations takes place. Hence the simultaneously pressure fluctuations occurred at 0.95 s should be induced by bubble coalescence. Fan et al. [31] proposed a source of global pressure fluctuations induced by bubble coalescence. Yet no direct evidence has been reported either experimentally or

numerically for this kind of source of pressure fluctuations in fluidized beds. Note that the bubble coalescence takes place at the time of about 0.95 s, and it can be argued that this fluctuation of pressure signal is responsible for bubble coalescence. Apparently the Euler-Euler two-fluid model in this work can well predict the pressure fluctuation due to bubble coalescence. However, as shown in Fig. 12 (b), this pressure fluctuation is only detected at the elevations lower than 0.4 m, which is corresponding to the height of bubble coalescence. Therefore, from our simulation results, the bubble coalescence may not generate a global pressure

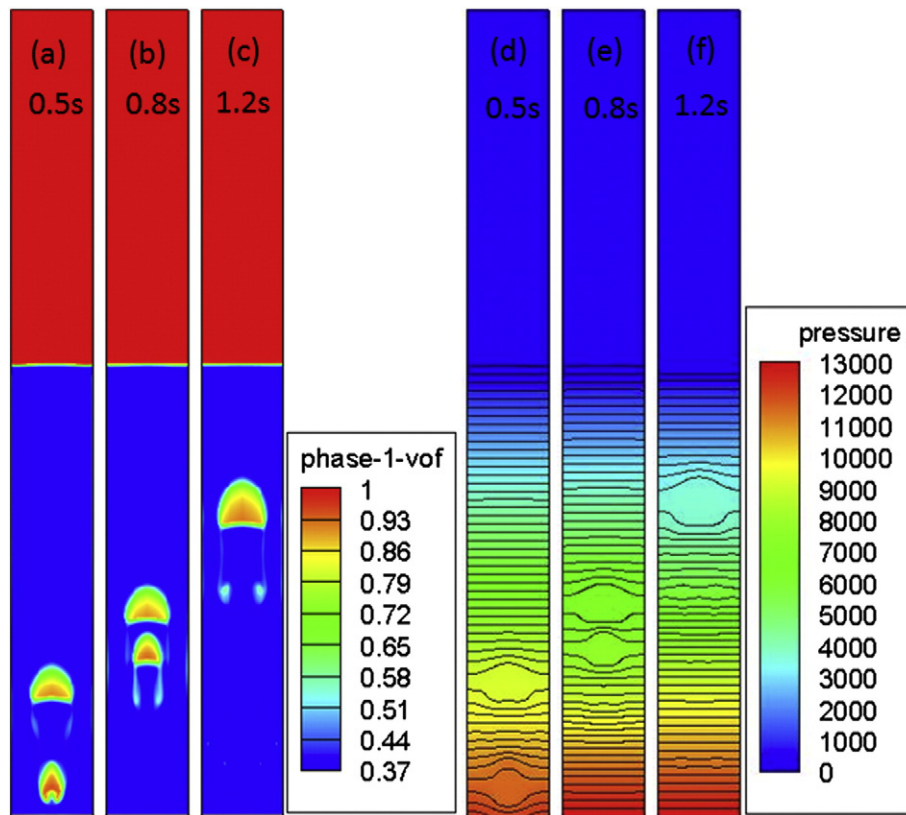


Fig. 11. The evolution of the gas voidage distribution (a–c) and the pressure field (d–f) in 2D fluidized bed (Reactor III: $W \times H$: 0.15 m \times 0.8 m) after two bubbles injected into the bed. The gas jet velocity is 6 m/s and jet duration is 0.1 s for the first bubble. The gas jet velocity is 6 m/s and jet duration is 0.08 s for the second bubble. And the time interval between these two bubbles is 0.25 s.

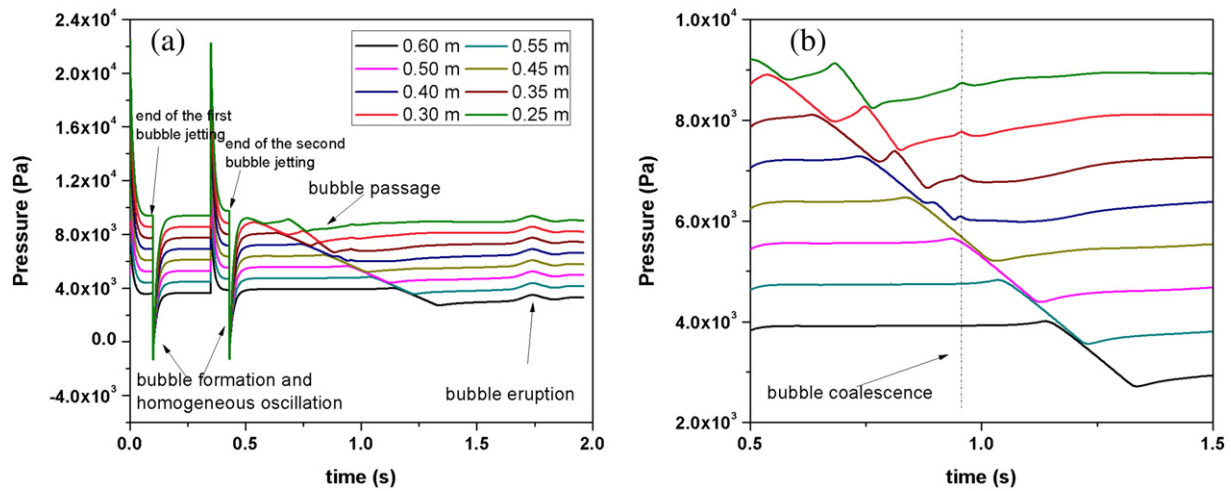


Fig. 12. (a) Time series of the normalized single-point pressure fluctuations at detected at different bed heights above the gas distributor in the 2D fluidized bed with twin-bubble rising (Reactor III: $W \times H$: 0.15 m \times 0.8 m); (b) Details of (a).

fluctuation, which is different from the pressure wave originated from bubble formation and eruption. The pressure fluctuation due to bubble coalescence can only be detected in the zone below the bubble coalescence point, implying a kind of semi-global pressure wave.

It can be seen from Fig. 12 that the detecting points can catch the local pressure signal induced by the two bubbles interchangeably. Taking the

bubble induced local pressure fluctuations at the bed height of 0.35 m as example, it can be found that the pressure signals from two successive bubbles are partly overlapped. The pressure curve from these two bubbles cannot be separated and the amplitude of the local pressure fluctuation differs significantly from that induced by a single bubble.

5.4. Discussions and comments on the pressure fluctuation analysis

Based on the simulation results of single-bubble rising or twin-bubble rising in fluidized beds, it becomes clear that the local bubble induced pressure fluctuation is dependent on the bubble size in a complicated way.

First of all, the simulation results suggest that the formation of bubble wake will complicate the quantitative bubble size estimation based on analysis of the local bubble induced pressure fluctuation. The formation of bubble wake will follow with a substantial change of bubble shape, and thereby the pressure field around a single bubble will change accordingly. The non-spherical nature of gas bubbles in fluidized beds will certainly cause systematic deviations the pressure field around a single bubble from the Davidson and Harrison model (cf. Fig. 8). Fig. 14 displays the pressure contours corresponding to the four conditions in Fig. 2. A comparative study between Fig. 2 and Fig. 14 visually shows that the pressure field around single bubble is dominant by the bubble shape. The bubble shape depends on the particle properties and operating conditions [32]. Kleijn van Willigen et al. [17] found different proportionality constants for different particle properties. The different bubble shape with different particle diameter may be one of the possible reasons.

On the second hand, the amplitude of the pressure fluctuation is not only a function of bubble size, but also affected by the lateral distance between the bubble and the detecting point, which has not been addressed in the spectral data decomposition method by van der Schaaf et al. Fig. 15 shows the time series of pressure signals at several bed heights in a bubbling fluidized bed, where Fig. 15 (a) corresponds to the detecting points at the vertical axis of the fluidized bed and Fig. 15 (b) at the wall. The synchronous signals marked at different bed heights in Fig. 15 are the global pressure waves (induced by bubble formation, bubble eruption, bubble coalescence etc.), while the lagging signals are the local bubble induced pressure fluctuations [10]. It can be seen from Fig. 9 that the amplitude of detected local pressure fluctuations decreases with increasing the radial distance between the detecting point and the bubble centre. Similar phenomenon can be captured in Fig. 15: Taking the time at 0.45 s in Fig. 15 as example, the radial distance between the bubble (at the bed height of about 0.4 m) and the detecting points at the bed vertical axis is much smaller than that between the bubble and the detecting points at the wall, and thereby the pressure

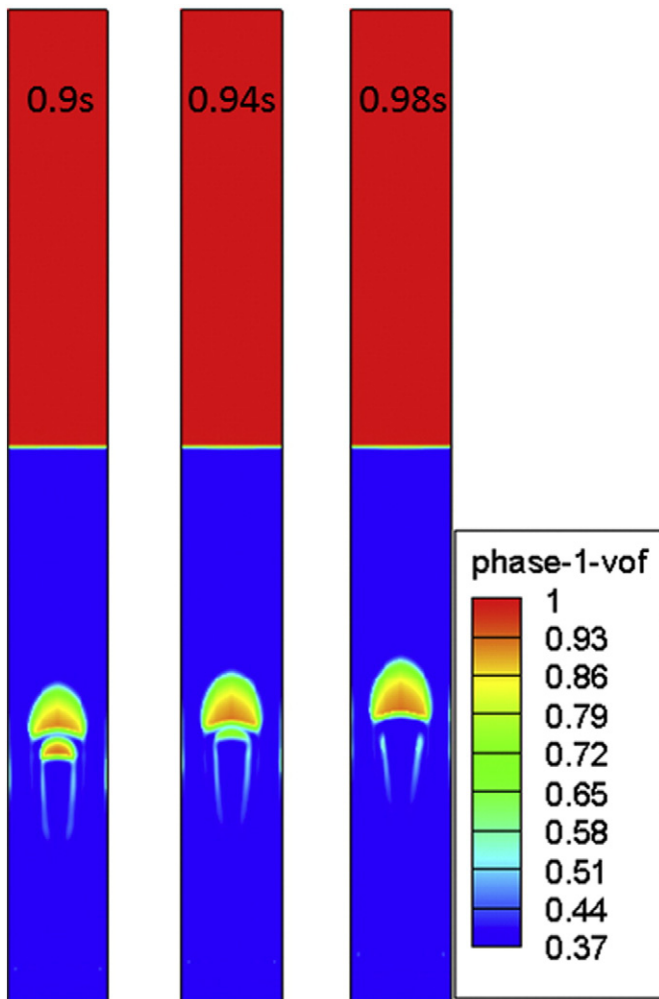


Fig. 13. Process of twin-bubble coalescence.

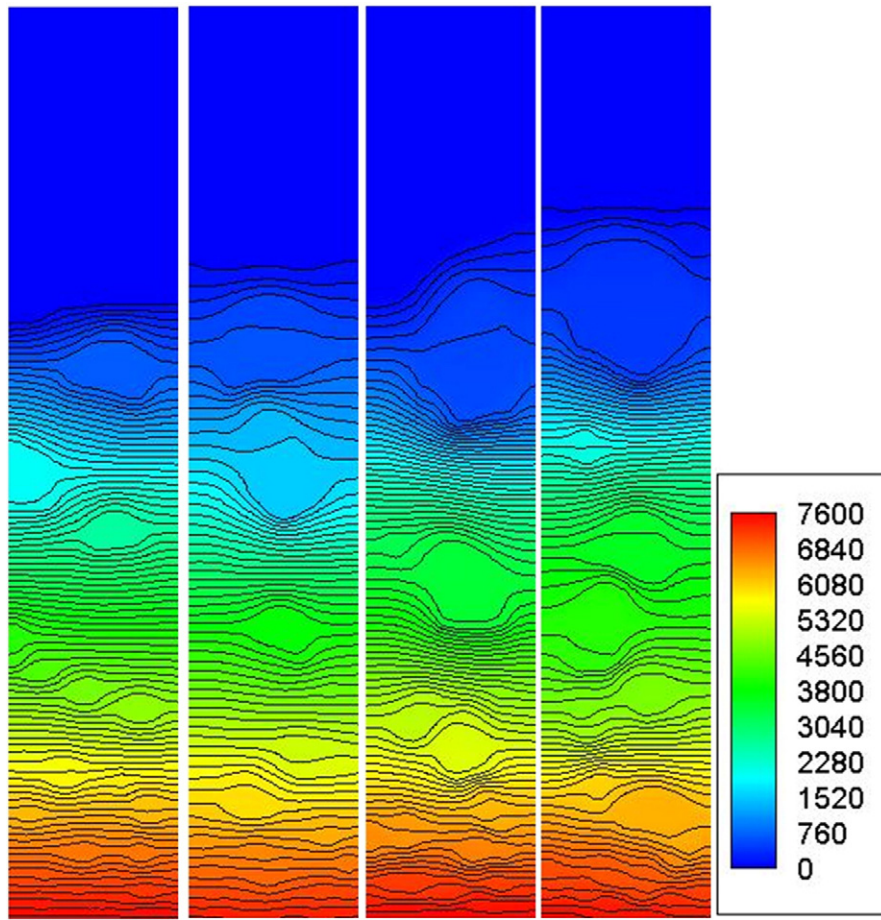


Fig. 14. Snapshots of pressure field in Reactor I ($W \times H$: 0.15 m \times 0.8 m) at different superficial velocities: (a) $U - U_{mf} = 0.08$ m/s, (b) $U - U_{mf} = 0.13$ m/s, (c) $U - U_{mf} = 0.18$ m/s, (d) $U - U_{mf} = 0.23$ m/s.

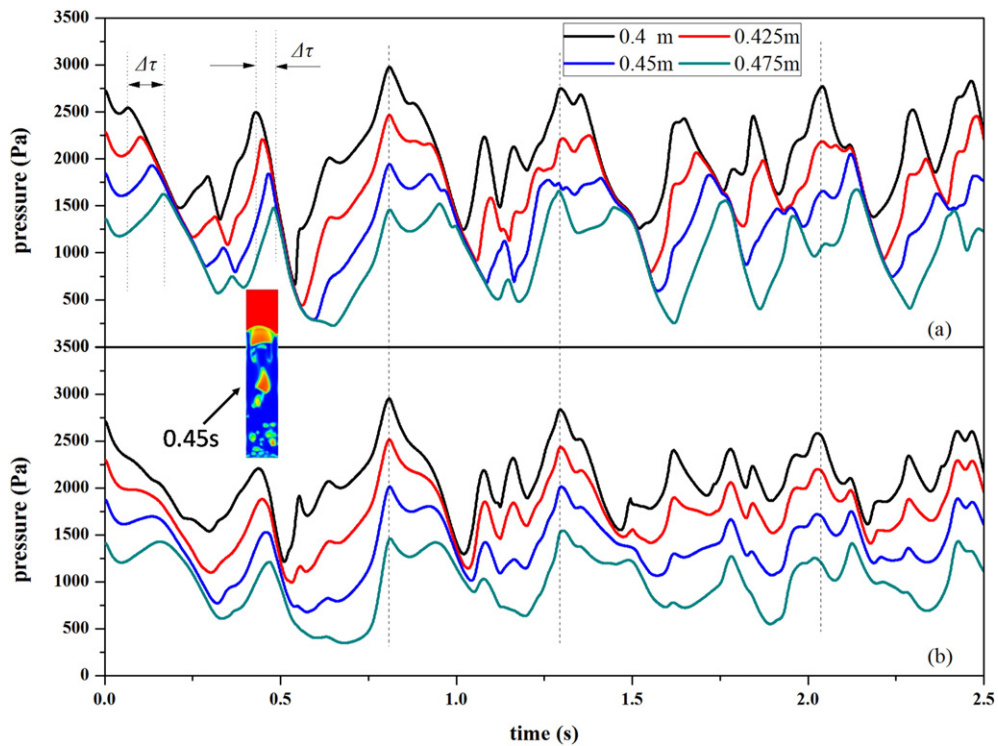


Fig. 15. Time series of pressure signals at different bed heights above the gas distributor in a bubbling fluidized bed: (a) in the centre axis of the bed; (b) on the wall.

fluctuations detected at the bed vertical axis is larger than that at the wall. In the bubbling fluidized beds, the bubble series randomly appear at the bed cross section, followed with a distribution of radial distance between the bubble centre and the detecting points. In the simulation cases of bubbling fluidized bed in this study (cf. Fig. 2), most of the time there is only one bubble passing by the bed cross section above 0.2 m. Hence the average radial distance between the bubble series and the detecting points is smaller in case of higher superficial velocity, contributing to the different proportional constant in Fig. 5 (b). Obviously the detecting point far away from the bubble will lead to the underestimation of bubble size. It is therefore necessary to include the influence of lateral position of the detecting points of pressure when analyzing the bubble size from pressure fluctuation signal.

Thirdly, the proportionality constant, is related to both the bubble size and the reactor size. When a bubble passes by the detecting zone, a portion of bed material will moving down to compensate the volume left bubble the bubble, leading to a decrease in the local pressure. For the same bubble size (thus the same amount of bed material), a larger bed will have a lower pressure fluctuation as the ratio of the weight of the bed material to the cross sectional area is lower (cf. Eq. (12)). More specifically, for the same bubble size, 2D fluidized bed and 3D fluidized bed are also expected to manifest different local pressure fluctuation following the Eq. (12). The size and shape of the fluidized bed in the literatures are different from each other, bringing about divers proportionality constant accordingly. Moreover, the proportionality constant is also related the bubble size in the same reactor, giving rise to the varying pattern of proportionality constant as displayed Fig. 10 (b) and Fig. 5 (b).

The results for the coalescence of two successive bubbles demonstrate that the local pressure waves induced by the passage of two successive bubbles will have certain overlap, which in turn affect the amplitude of the local pressure fluctuations. Note that the duration of the overlap is relative to the bubbling frequency. Actually it was found that the bubbling coalescence frequency along the bed height is different for Geldart A, B, and D particles [33]. The difference between the bubbling coalescence frequency may be also responsible for to the scattered proportionality constant in the experiments by Kleijn van Willigen et al. [17].

The results obtained in this work can be used as guidance for further improving the pressure fluctuation analysis based on the frequency decomposition method for bubble size estimation. The improvement can be made in several aspects. Firstly, the influence of lateral distance between the detecting point and bubble axis needs to be accounted for. Secondly, the influence of reactor size on the local pressure fluctuations should be added. Thirdly, the bubble coalescence will also be considered. Apparently the ignorance of these sources will lead to significant systematic deviation in bubble size estimation.

Further experimental work is desired to confirm this finding. A pressure fluctuation analysis method on the basis of the spectral data decomposition method accounting for above points is under development by the authors and will be subject to another publication. Anyway, it is always important to carry out a careful calibration of the bubble equivalent size by well-developed measurement methods such as ECT, optical probes, etc., before the use of validated pressure fluctuation analysis for bubble size estimation.

6. Conclusions

From the numerical simulations of bubbling fluidized beds, it can be found that the bubble size predicted by the spectral data decomposition method by van der Schaaf et al. [12] can be much smaller than the real one, and the proportionality constant increases with the decrease of bubble size. By comparing the incoherent output PSD with that of the local solid holdup signals, it can be found that, with the existing spectral decomposition method, the local bubble induced pressure fluctuation can be successfully separated from the global pressure waves. The underlying reasons of the scattered

proportionality constants can be well explained by the rising of a single bubble or twin bubbles in a fluidized bed at minimum fluidization condition. The size of bubble can be carefully controlled by altering gas velocity through the center jetting orifice. It has been shown that the local bubble induced pressure fluctuation is not only a function of bubble size, but also affected by bubble shape, the lateral distance between bubble and the detecting point, bed diameter, and bubble coalescence. The spectral data decomposition method is subject to larger deviation because the points discussed above are not considered. The results obtained in this work are expected to help us to improve the pressure fluctuation analysis method for accurate bubble size estimation.

Nomenclature

P_r	relative pressure (Pa)
g	gravity acceleration (m/s^2)
R_b	bubble radius (m)
R_B	bed radius (m)
r	angle coordinate (m)
\vec{u}_g	gas velocity (m/s)
u_s	solid velocity (m/s)
p	pressure (Pa)
ρ_p	particle diameter (m)
Re	particle Reynolds number (—)
C_{XY}	coherence (—)
L_b	bubble size (or characteristic length scale) by the spectral data decomposition method (m)
l_b	bubble size (or characteristic length scale) from local pressure fluctuations due to bubble passage (m)
D_b	bubble diameter (m)
A	total area occupied by a 2D bubble (m^2)
V	total volume occupied by a 3D bubble (m^3)
\bar{D}_b	average bubble diameter (m)
X	lateral distance between the detecting point and the bubble center (m)
Z	vertical distance between the detecting point and the bubble center (m)
h	height above the gas distributor (m)
A_o	area of distributor per orifice (m^2)
U	superficial velocity (m/s)

Greek symbols

μ_g	gas viscosity (Pa·s)
ρ_p	particle density (kg/m^3)
ρ_g	gas density (kg/m^3)
σ	standard deviation (Pa)
ε	voidage (—)
β	inter-phase momentum transfer coefficient ($kg/m^3/s$)
$\bar{\tau}_g$	gas phase stress tensor (Pa)
$\bar{\tau}_s$	solid phase stress tensor (Pa)
ϑ	granular temperature (m^2/s^2)
γ_s	diffusion coefficient for granular energy (m^2/s^3)
δ	depth of a pseudo 2D fluidized bed (m)
θ	angle coordinate (rad)

Subscripts and superscripts

e	emulsion or dense phase
g	gas
mf	minimum fluidization condition
p	particle
b	bubble
B	bed
s	solid
r	relative

Acknowledgements

This work is supported by the National Natural Science Foundation of China (Grant No. 91334205) and the National Science Fund for Distinguished Young Scholars (Grant No. 51525601).

References

- [1] J. Xue, M. Al-Dahhan, M. Dudukovic, R. Mudde, Four-point optical probe for measurement of bubble dynamics: validation of the technique, *Flow Meas. Instrum.* 19 (2008) 293–300.
- [2] D. Tayebi, H.F. Svendsen, A. Grisingås, T. Mejdell, K. Johannessen, Dynamics of fluidized-bed reactors. Development and application of a new multi-fiber optical probe, *Chem. Eng. Sci.* 54 (1999) 2113–2122.
- [3] R. Mudde, Bubbles in a fluidized bed: a fast X-ray scanner, *AIChE J.* 57 (2011) 2684–2690.
- [4] R.F. Mudde, Time-resolved X-ray tomography of a fluidized bed, *Powder Technol.* 199 (2010) 55–59.
- [5] I. Hulme, A. Kantzas, Determination of bubble diameter and axial velocity for a polyethylene fluidized bed using X-ray fluoroscopy, *Powder Technol.* 147 (2004) 20–33.
- [6] H. Wang, W. Yang, P. Senior, R. Raghavan, S. Duncan, Investigation of batch fluidized-bed drying by mathematical modeling, CFD simulation and ECT measurement, *AIChE J.* 54 (2008) 427–444.
- [7] S. Liu, W. Yang, H. Wang, F. Jiang, Y. Su, Investigation of square fluidized beds using capacitance tomography: preliminary results, *Meas. Sci. Technol.* 12 (2001) 1120.
- [8] H.T. Bi, A critical review of the complex pressure fluctuation phenomenon in gas-solids fluidized beds, *Chem. Eng. Sci.* 62 (2007) 3473–3493.
- [9] H. Bi, J. Grace, J. Zhu, Propagation of pressure waves and forced oscillations in gas-solid fluidized beds and their influence on diagnostics of local hydrodynamics, *Powder Technol.* 82 (1995) 239–253.
- [10] J. Van der Schaaf, J. Schouten, C. Van den Bleek, Origin, propagation and attenuation of pressure waves in gas-solid fluidized beds, *Powder Technol.* 95 (1998) 220–233.
- [11] J.F. Davidson, *Fluidized Particles*, Springer, 1995.
- [12] J. Van der Schaaf, J. Schouten, F. Johnsson, C. Van den Bleek, Non-intrusive determination of bubble and slug length scales in fluidized beds by decomposition of the power spectral density of pressure time series, *Int. J. Multiphase Flow* 28 (2002) 865–880.
- [13] M. Liu, Y. Zhang, H. Bi, J.R. Grace, Y. Zhu, Non-intrusive determination of bubble size in a gas-solid fluidized bed: an evaluation, *Chem. Eng. Sci.* 65 (2010) 3485–3493.
- [14] L. van der Lee, B. Chandrasekaran, I. Hulme, A. Kantzas, A non-invasive hydrodynamic study of gas-solid fluidized bed of linear low density polyethylene, *Can. J. Chem. Eng.* 83 (2005) 119–126.
- [15] Y. Zhang, H.T. Bi, J.R. Grace, C. Lu, Comparison of decoupling methods for analyzing pressure fluctuations in gas-fluidized beds, *AIChE J.* 56 (2010) 869–877.
- [16] M. Rüdüsüli, T.J. Schildhauer, S.M. Biollaz, A. Wokaun, J.R. van Ommen, Comparison of bubble growth obtained from pressure fluctuation measurements to optical probing and literature correlations, *Chem. Eng. Sci.* 74 (2012) 266–275.
- [17] F. Kleijn van Willigen, J.R. van Ommen, J. van Turnhout, C. van den Bleek, Bubble size reduction in a fluidized bed by electric fields, *Int. J. Chem. React. Eng.* 1 (2003).
- [18] D. Gidaspow, *Multiphase Flow and Fluidization: Continuum and Kinetic Theory Descriptions*, Academic press, 1994.
- [19] C. Lun, S.B. Savage, D. Jeffrey, N. Chepurini, Kinetic theories for granular flow: inelastic particles in Couette flow and slightly inelastic particles in a general flowfield, *J. Fluid Mech.* 140 (1984) 223–256.
- [20] A. Boemer, H. Qi, U. Renz, Eulerian simulation of bubble formation at a jet in a two-dimensional fluidized bed, *Int. J. Multiphase Flow* 23 (1997) 927–944.
- [21] P. Witt, J. Perry, M. Schwarz, A numerical model for predicting bubble formation in a 3D fluidized bed, *Appl. Math. Model.* 22 (1998) 1071–1080.
- [22] P.C. Johnson, R. Jackson, Frictional-collisional constitutive relations for granular materials, with application to plane shearing, *J. Fluid Mech.* 176 (1987) 67–93.
- [23] C. Wen, Y. Yu, *Mechanics of fluidization*, Chem. Eng. Prog. Symp. Ser. (2013) 100.
- [24] S. Ergun, Fluid flow through packed columns, *Chem. Eng. Prog.* 48 (1952) 89–94.
- [25] J. Sinclair, R. Jackson, Gas-particle flow in a vertical pipe with particle-particle interactions, *AIChE J.* 35 (1989) 1473–1486.
- [26] R. Darton, Bubble growth due to coalescence in fluidized beds, *Chem. Eng. Res. Des.* 55 (1977) 274–280.
- [27] P. Cai, M. Schiavetti, G. De Michele, G. Grazzini, M. Miccio, Quantitative estimation of bubble size in PFBC, *Powder Technol.* 80 (1994) 99–109.
- [28] L. Shen, F. Johnsson, B. Leckner, Digital image analysis of hydrodynamics two-dimensional bubbling fluidized beds, *Chem. Eng. Sci.* 59 (2004) 2607–2617.
- [29] H. Littman, G.A. Homolka, The pressure field around a two-dimensional gas bubble in a fluidized bed, *Chem. Eng. Sci.* 28 (1973) 2231–2243.
- [30] V. Chilekar, M. Warnier, J. Van Der Schaaf, B. Kuster, J. Schouten, J. Van Ommen, Bubble size estimation in slurry bubble columns from pressure fluctuations, *AIChE J.* 51 (2005) 1924–1937.
- [31] L.T. Fan, T.-C. Ho, S. Hiraoka, W.P. Walawender, Pressure fluctuations in a fluidized bed, *AIChE J.* 27 (1981) 388–396.
- [32] W.-C. Yang, *Handbook of Fluidization and Fluid-Particle Systems*, CRC press, 2003.
- [33] J.-H. Choi, J.-E. Son, S.-D. Kim, Generalized model for bubble size and frequency in gas-fluidized beds, *Ind. Chem. Res.* 37 (1998) 2559–2564.